Earth and Planetary Science Letters 530 (2020) 115947

Contents lists available at ScienceDirect

Earth and Planetary Science Letters

www.elsevier.com/locate/epsl

Unravelling the sources of carbon emissions at the onset of Oceanic Anoxic Event (OAE) 1a

Markus Adloff [a,*], Sarah E. Greene [b], Ian J. Parkinson [c], B. David A. Naafs [d,c], Will Preston [c], Andy Ridgwell [e,a], Dan J. Lunt [a], José Manuel Castro Jiménez [f], Fanny M. Monteiro [a]

[a] School of Geographical Sciences, University of Bristol, University Road, BS81SS, UK
[b] School of Geography, Earth and Environmental Sciences, University of Birmingham, Edgbaston, B152TT, UK
[c] School of Earth Sciences, University of Bristol, Queen's Road, BS81RJ, UK
[d] School of Chemistry, University of Bristol, Cantock's Close, BS81TS, UK
[e] Department of Earth Sciences, University of California Riverside, 900 University Ave, Riverside, CA 92521, USA
[f] Departamento de Geología, CEACTierra, Universidad de Jaén, Campus Las Lagunillas s/n, 23071 Jaén, Spain

ARTICLE INFO

Article history:
Received 7 March 2019
Received in revised form 7 October 2019
Accepted 3 November 2019
Available online 15 November 2019
Editor: I. Halevy

Dataset link:
https://github.com/derpycode/cgenie.muffin

Keywords:
Aptian
data assimilation
carbon source
osmium isotopes
volcanism

ABSTRACT

The early Aptian Oceanic Anoxic Event (OAE) 1a represents a major perturbation of the Earth's climate system and in particular the carbon cycle, as evidenced by widespread preservation of organic matter in marine settings and a characteristic negative carbon isotopic excursion (CIE) at its onset, followed by a broad positive CIE. The contemporaneous emplacement of a large igneous province (LIP) is invoked as a trigger for OAE 1a (and OAEs in general), but this link and the ultimate source of the carbon perturbation at the onset of OAEs is still debated. In this study, we simultaneously assimilate an atmospheric pCO_2 reconstruction along with a $\delta^{13}C$ record from the Spanish Cau section in an Earth system model to obtain a novel transient reconstruction of emission rates and identify the primary carbon-emitting sources across the negative CIE interval at the onset of OAE 1a. We reconstruct carbon emissions of 4,300–29,200 Pg from a mixture of carbon sources. This estimate is a lower bound, as contemporaneous organic carbon burial is not accounted for. Carbon was first released at slow rates from a ^{13}C-depleted reservoir (e.g. thermo- and/or biogenic methane from sill intrusions). Towards the end of the negative CIE the rate of emissions increased and they became more ^{13}C-enriched, likely from a dominantly volcanic source (e.g. LIPs). New osmium isotope ($^{187}Os/^{188}Os$) measurements, from the same section as the pCO_2 reconstruction and $\delta^{13}C$ data, reveal a shift to less radiogenic values coinciding with the change towards mantle-derived carbon emissions as indicated by our modelling results, lending further support to our interpretation. These results highlight that geologically triggered carbon emissions were likely driving the OAE onset.

1. Introduction

The early Aptian Oceanic Anoxic Event (OAE) 1a (~121 Ma, Olierook et al., 2019) represents one of the largest perturbations of the climate system during the last 200 Myr (Jenkyns, 2010). Although OAEs, including OAE 1a, were first identified in the 1970s (Schlanger and Jenkyns, 1976), it is still unclear exactly how the oceanic system evolved into such an extreme state. Increasing nutrient supply to the photic zone and, to a lesser extent, climate warming may have played a crucial role (Larson and Erba, 1999; Jenkyns, 2010; Monteiro et al., 2012), driving increased productivity and subsurface oxygen demand, and reduced oxygen solubility, respectively. The resulting reduced oceanic oxygen concentrations would have led to enhanced preservation and burial of organic matter (Jenkyns, 2010; Monteiro et al., 2012). However, the driver of this warming and increased nutrient delivery is debated.

While all OAEs are associated with a positive carbon isotopic excursion (CIE), interpreted as reflecting an interval of enhanced burial of organic matter, the onset of OAE 1a is characterized by a distinct negative CIE prior to the positive CIE (Menegatti et al., 1998). Because of the broad temporal coincidence of OAE 1a with the emplacement of the Ontong-Java Plateau, the negative CIE could have resulted from carbon input from (submarine) volcanism initiating the OAE by warming the climate and releasing nutrients to the ocean (e.g. Weissert, 1989). A phase of increased volcanism during the onset of OAE 1a (and other OAEs) is further highlighted

* Corresponding author.
E-mail address: markus.adloff@bristol.ac.uk (M. Adloff).

https://doi.org/10.1016/j.epsl.2019.115947

by the observed perturbations of the marine osmium cycle (Tejada et al., 2009; Bottini et al., 2012). However, it is not certain whether volcanic emissions could have caused the negative CIE, so destabilization of methane hydrates has been proposed as an alternative, more ^{13}C-depleted carbon source (Beerling et al., 2002; van Breugel et al., 2007; Méhay et al., 2009; Malinverno et al., 2010).

Constraining the carbon source for OAE 1a is crucial as it has implications for the mass and rate of carbon emissions and hence extent of the perturbation estimated from the carbon isotope record. The size of a negative CIE is a function of the mass of emitted carbon and its isotopic composition (e.g. Kirtland-Turner and Ridgwell, 2016), a predominantly volcanic carbon source (CO_2), relatively enriched in ^{13}C compared to organic carbon sources, requires massive carbon emissions to match the negative CIE, resulting in high atmospheric CO_2 concentrations (e.g. 3000 ppm pCO_2 increase (Bauer et al., 2017)). In contrast, the estimated emissions, and hence CO_2 concentrations, are much lower if the carbon originated predominantly from more ^{13}C-depleted sources (e.g. 600 ppm for methane emissions (Beerling et al., 2002)).

The nature of the dominant carbon source is important to determine the role of Earth system feedbacks in triggering OAE formation in the Aptian and its sensitivity to carbon injections. For instance, predominant volcanic CO_2 emissions suggest OAE formation was primarily a response to external forcing while a dominant biogenic methane source would indicate a major role for feedbacks between surface carbon reservoirs and an increased sensitivity to carbon emissions. This could have broader implications for our understanding of the formation of other Mesozoic OAEs since negative CIEs are also known from OAE 1b and the Toarcian OAE, and the presence of a suppressed negative CIE before OAE 2 is discussed (Jenkyns, 2010).

Recently, a continuous pCO_2 proxy record across OAE 1a (Naafs et al., 2016) together with a $\delta^{13}C_{carb}$ record from the same site provides an opportunity to identify the carbon source and quantify emissions rates across OAE 1a. The pCO_2 record, based on compound-specific and bulk $\delta^{13}C_{carb}$ from the hemipelagic Tethyan Cau section, shows a gradual pCO_2 increase during the negative CIE starting around 800–1000 ppm and reaching maximum values of 2000 ± 1200 ppm before the recovery of the negative CIE. This estimate is within the range of previously reconstructed pCO_2 values during the Early Cretaceous of 200–2000 ppm (see Wang et al., 2014, for a compilation) and is between pCO_2 values predicted for a pure methane and a purely volcanic source. At the same time as the pCO_2 increase, organic proxies indicate a 2–5 °C increase in local sea-surface temperature (SST) during the negative CIE (Mutterlose et al., 2014; Naafs and Pancost, 2016). Global temperature changes of this magnitude are consistent with a doubling to quadrupling of pCO_2, depending on assumptions about the initial pCO_2 and the climate sensitivity of the Early Cretaceous. At the same time, biological turn-over and carbonate platform drowning, key features of OAE 1a, have been interpreted as being the results of surface ocean acidification due to increased pCO_2 (Wissler et al., 2003; Erba et al., 2010). However, it is debated whether the relative timing, the amount, and the rate of emitted carbon explain the observed changes (Gibbs et al., 2011; Naafs et al., 2016).

In this study, we assimilate the observed negative CIE and reconstructed pCO_2 changes from the Cau section in the Earth system model cGENIE (Ridgwell et al., 2007) to constrain carbon emissions across the onset of OAE 1a and to understand their implications for the dominant carbon sources. We also assess the effect of the pCO_2 changes on Earth's climate, as well as quantifying the implications of uncertainties in pCO_2 change estimates and duration of the OAE onset for reconstructing the carbon cycle perturbation. Finally, we compare our simulation results to a newly-generated osmium isotope record from the same section, which allows us to reconsider the relationship between the negative CIE and environmental perturbations at the onset of OAE 1a.

2. Methods

2.1. The Cau section

The studied succession belongs to the Almadich Formation, made of a cyclic succession of hemipelagic marls and marsltones of late Barremian- Aptian p.p. age (Aguado et al., 1999; Castro et al., 2008). The interval considered in this study is located in the upper part of the lower member of the Almadich Formation, of Early Aptian age (Desayesites forbesi ammonite zone, B. blowi planktonic foraminifera, see Naafs et al., 2016). The lithologies present are dominant grey marls (beds 0.5–2.5 m thick) alternating with marly limestones (beds 0.3–0.6 m thick), with two levels of dark marls (ca. 0.4 m thick) containing small pyrite nodules. The samples used for Os analyses were taken from the marly limestone levels, that have a $CaCO_3$ content between 36 and 70% wt and TOC contents ranging from $<$0.7 to 2.4% wt. We assume stratigraphic continuity and a constant sedimentation rate as there is no sedimentological evidence for interruption of sedimenation (hard/soft-ground or erosive surfaces). Also biostratigraphy and nannofossils associations are consistent with a continuous record, at the scale of the resolution available (Aguado et al., 1999; Naafs et al., 2016).

2.2. Model setup and experiment design

cGENIE is the carbon cycle centric version of the Grid ENabled Integrated Earth system model (GENIE), which couples a 3D ocean with a 2D zonally-averaged atmosphere (Edwards and Marsh, 2005), accounting for the biogeochemical cycles of carbon, phosphorus, sulphur, oxygen and stable carbon isotopes (Ridgwell et al., 2007). cGENIE can be run with a vertically-integrated sediment module which builds up deep sea sediments with varying $CaCO_3$ content and carbon isotopic composition, resolving for $CaCO_3$ burial and dissolution (Ridgwell and Hargreaves, 2007) and with a terrestrial weathering module (Colbourn et al., 2013) hence closing the geological carbon cycle. Its design also allows for inversion (data assimilation) experiments (e.g. Cui et al., 2011; Gutjahr et al., 2017, see below).

Here we ran the model on a 36x36 grid with 16 vertical levels in the ocean, and included modules for weathering and marine sediments by which alkalinity is added to or removed from the ocean.

In our model set-up, carbon emissions affect temperature, weathering rates, ocean solubility of gases, and ocean circulation. Wind fields are fixed and prescribed as boundary conditions and hence do not change in response to changing atmospheric CO_2 concentration and greenhouse warming.

We configured cGENIE for the early Aptian using paleogeography and bathymetry (see Appendix A), wind fields, and planetary albedo from the Aptian modelling setup of Donnadieu et al. (2006). Temperature effects on biogeochemical production were included, and remineralization profiles adapted to a warmer ocean (John et al., 2014). We spun up the model in a first step (20 kyr) to equilibrate to an atmospheric CO_2 concentration of 840 ppm (as reconstructed for the start of the negative CIE in Naafs et al. (2016)) and atmospheric δ^{13}C value of $-6‰$, which is at the upper limit of measured values of the modern atmospheric composition (Craig, 1953). Carbonate production is set up as in Ridgwell and Schmidt (2010) to represent a warm, ice-free world. We assume that organic carbon burial did not play a major role for the marine carbon cycle during the interval that we simulate here (see Discussion section), but in order to equilibrate oceanic δ^{13}C in the absence of organic carbon burial, we set the carbon isotopic composition

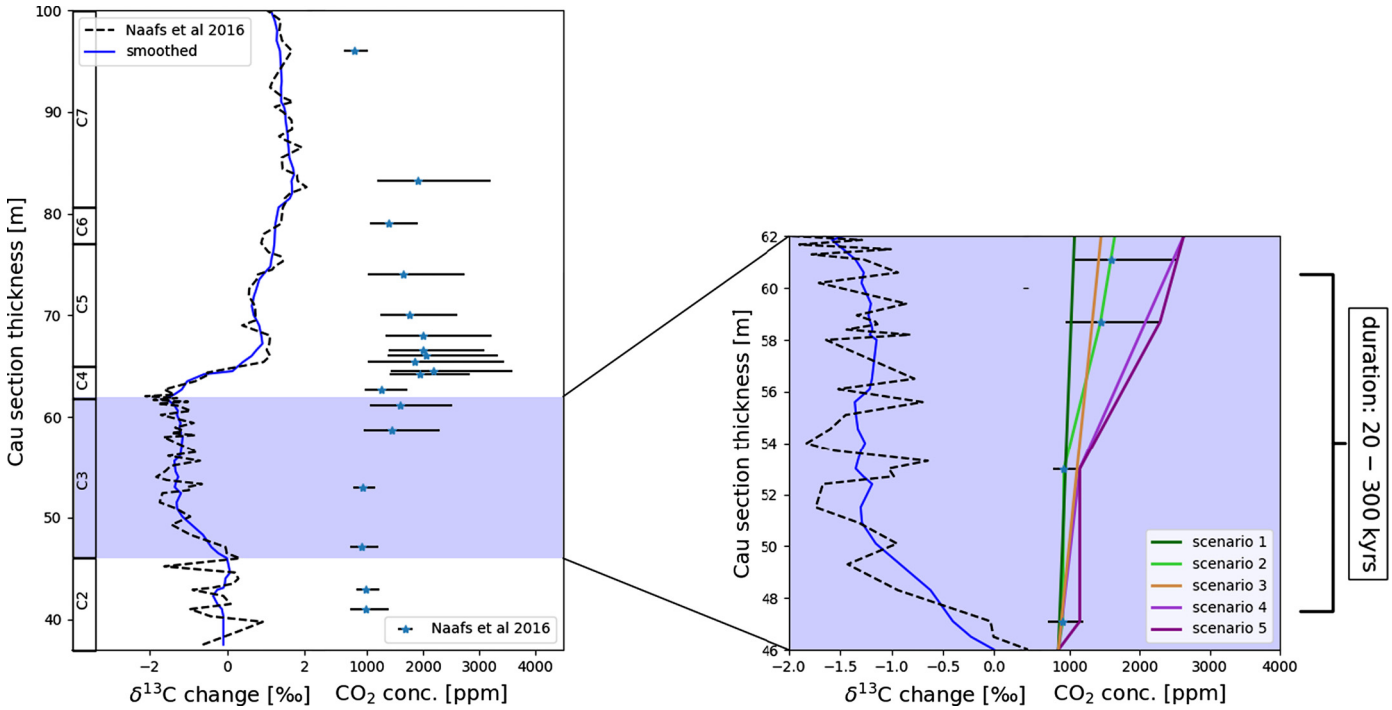

Fig. 1. Reconstructed properties of the surficial carbon reservoir during OAE 1a (segments after Naafs et al. (2016)) and pCO_2 forcings used in this study. a) Reconstruction of bulk carbonate $\delta^{13}C$ variation and pCO_2 across OAE 1a based on proxy data from Cau (Naafs et al., 2016): b) Zoom into the onset of the negative CIE, showing $\delta^{13}C$ changes and the 5 pCO_2 scenarios we tested in cGENIE. $\delta^{13}C$ values are given as offsets from the highest value in the smoothed $\delta^{13}C_{carb}$ data series prior to the start of OAE 1a. (For interpretation of the colours in the figure(s), the reader is referred to the web version of this article.)

of the weathering flux to 6.2‰. Initial calcium ion supply from terrestrial weathering is set to 34 Pmol yr^{-1}, resulting in an average surface calcite saturation state (4.3) within the reconstructed range for the Early Cretaceous (Ridgwell and Zeebe, 2005). The initial oceanic nutrient inventory was set to 1.06 µmol PO_4^{3-} kg^{-1} ocean water, equalling half of the preindustrial oceanic phosphate inventory. This is based on a model-data comparison of pre-OAE 1a anoxia extents, following Monteiro et al., 2012 (see appendix G). However, sensitivity experiments showed that the initial phosphate inventory has little effect on our results (see fig. D2 in the appendix). During the second spin up stage (500 kyr), the model was run as an open system so that volcanic outgassing, riverine input of solutes to the ocean, and carbonate burial in marine sediments could reach equilibrium.

To constrain carbon fluxes and their isotopic composition across OAE 1a onset, we used a double data assimilation approach. Similar studies with single assimilations used the size of negative CIEs to constrain emission rates associated with other major carbon cycle events such as the Paleocene-Eocene Thermal Maximum (PETM, e.g. Cui et al., 2011; Turner and Ridgwell, 2013) making assumptions about the $\delta^{13}C$ signature of the carbon source. Here however, we intend to reconstruct both the mass and provenance (i.e. isotopic composition) of the emitted carbon. Knowing that a given isotopic excursion can be produced by adding a small mass of very ^{13}C-depleted carbon or a large mass of less ^{13}C-depleted carbon (e.g. Kirtland-Turner and Ridgwell, 2016) this constitutes a problem with two unknowns (mass and composition), the solution for which requires an additional constraint to the CIE size. We hence combined estimates of atmospheric $\delta^{13}C$ changes with estimates of pCO_2 changes (Naafs et al., 2016) to reconstruct carbon emissions across the onset of the OAE 1a negative CIE.

Each time step, cGENIE adds the mass of carbon needed to reach the prescribed pCO_2 target to the atmosphere, and then calculates the required isotopic signature of that carbon addition to create the right CIE. We allow a maximum carbon emission rate of 10 Pg yr^{-1} with a $\delta^{13}C$ not more negative than −100‰. We used the Naafs et al. (2016) pCO_2 estimates based on $\Delta^{13}C$, the offset between compound specific $\delta^{13}C$ in organic matter and bulk carbonate $\delta^{13}C$ ($\delta^{13}C_{carb}$) (Popp et al., 1998). We assumed that the evolution of $\delta^{13}C_{carb}$ reflects marine and atmospheric $\delta^{13}C$ changes (see Appendix C). For this, we correct sedimentary $\delta^{13}C$ measurements from the Cau section by applying a 7.7‰ offset to account for different baseline $\delta^{13}C$ values between atmosphere and biogenic $CaCO_3$. We smooth these data by applying a running mean over 7 data points (see Fig. 1) to minimize the effect of short-term fluctuations. This smoothed sedimentary $\delta^{13}C$ is characterized by an averaged 1.3‰ negative excursion (maximum value 1.6‰), which is similar to most other measured negative CIE amplitudes for OAE 1a (see Appendix B). This dual data assimilation exercise is analogous to Gutjahr et al. (2017)' assessment of the PETM carbon cyle perturbation, except here taking pelagic $\delta^{13}C_{carb}$ as a measure of atmospheric rather than surface ocean (DIC) $\delta^{13}C$ changes, and we directly constrain the rate of emissions using a pCO_2 reconstruction rather than surface pH.

We additionally address a number of uncertainties in the data and its interpretation. Firstly, implications of uncertainties in the pCO_2 reconstruction are explored by using an ensemble of 5 simulations with different pCO_2 trajectories within the uncertainty envelope reconstructed by Naafs et al. (2016) (Fig. 1). This uncertainty envelope accounts for uncertainties in the calibration of the pCO_2 reconstruction method to Cretaceous organisms and due to the fluctuability of the ^{13}C curve in Cau outcrop data. Secondly, the duration of the negative CIE at the OAE 1a onset is poorly constrained. We run every pCO_2 scenario with a duration of 100 kyr, but since durations between 20 and 300 kyr have been suggested for the onset of the negative CIE interval (e.g. van Breugel et al., 2007; Li et al., 2008; Malinverno et al., 2010; Hu et al., 2012), we repeat some simulations with three different assumed durations: 20 kyrs, 40 kyrs and 300 kyrs. In total, we run 20 inverse modelling simulations, exploring 5 different pCO_2 trajectories and 4 different assumptions about durations. Additional sensitivity

experiments were run to investigate the sensitivity to boundary conditions (see Appendix).

2.3. Osmium isotope analysis

Osmium (Os) isotopes and Os and Rhenium (Re) concentrations were determined at the School of Earth Sciences, University of Bristol. Samples were digested in Carius tubes using techniques slightly modified from Shirey and Walker (1995). 0.3–0.5 g of powder was added to the Carius tubes. As the rock contained a significant amount of carbonate (46 m – 62 m of the Cau section consist of a succession of marl and marly limestone, see Quijano et al. (2012) and Naafs et al. (2016) for more information on the lithologies) the powder was decarbonated with a small amount of concentrated HCl prior to sealing. Appropriate amounts of ^{190}Os and ^{185}Re spikes were added to the Carius tubes along with additional HCl and HNO_3 to make up 12 ml of inverse aqua regia. The samples were then digested at 230 °C for 48 hours. This technique recovers hydrogenic Os and Re without dissolving any detrital material.

Os and Re separation chemistry and mass spectrometry follows methods recently described in detail elsewhere (Josso et al., 2019). For Os isotope analyses the purified Os was analysed on a ThermoFisher Triton thermal ionisation mass spectrometer (TIMS) in N-TIMS mode, with instrumental mass fractionation corrected for using the exponential mass fractionation law and a ^{192}Os/^{188}Os ratio of 3.08271. Os concentrations were determined by isotope dilution and the isotope data were spike-stripped to yield the sample ^{187}Os/^{188}Os ratio. Total procedural blanks were determined for each dissolution batch and yielded Os concentrations of 0.31 and 1.46 pg, with ^{187}Os/^{188}Os ratios of 0.1783 ± 0.0347 and 0.1745 ± 0.0557 respectively. All data were corrected for the procedural blank with blank corrections usually less than 1.5% (range 0.04 to 4%) on the concentration and usually less than 1% (range 0.02–3.5%) on the ^{187}Os/^{188}Os ratio depending on sample size and Os concentration. A DTM solution standard was run during the analytical period and yielded a ^{187}Os/^{188}Os ratio of 0.17396 ± 39 (2sd, $n = 12$), within error of previous determinations of the standard (e.g. Birck et al., 1997). Precision on the standard and samples is similar because they were both run at comparable beam intensity, with the exception of one sample, which has a precision of 12‰.

Re isotopes were measured by multi-collector inductively plasma source mass spectrometry (MC-ICP-MS) on a ThermoFisher Neptune using a SEM and corrected for instrumental mass fractionation using the exponential mass fractionation law and a ^{191}Ir/^{193}Ir ratio of 0.59418. Total procedural blanks were determined for each dissolution batch and yielded Re concentrations of 5 ± 2 pg, with Re concentrations determined by isotope dilution and blank corrected using the appropriate procedural blank. Blank corrections for the Re concentrations are less than 2% (range 0.14–4.1%). A 9 ppt solution of the NIST SRM3134 Re standard, doped with Ir, was run during the analytical period and yielded a ^{187}Re/^{185}Re ratio within error of previous determinations of the standard (Miller et al., 2009). One sample (Cau-21) was fully duplicated, because it had elevated Re concentrations, low Os concentrations and gave a low initial ^{187}Os/^{188}Os ratio at a key part of the section. The duplicate analyses gave initial ^{187}Os/^{188}Os ratios just outside of analytical uncertainty, but confirming that there is significant drop in initial ^{187}Os/^{188}Os ratio in the section at this time.

3. Results

The model simulations provide estimates of carbon emission rates and the isotopic composition of the emitted carbon for the onset of the Aptian negative CIE under different pCO_2 change scenarios (Fig. 2a-b) and onset durations (Fig. 2c-d). In our simulations, total emissions ranged between 4,300–29,200 Pg C with emission rates between 0.01 and 0.7 Pg C yr^{-1}. The uncertainty in our carbon emission estimates is almost equally attributable to uncertainties in the duration of the event and the pCO_2 reconstruction (10,300 Pg C and 13,700 Pg C respectively). Alternative assumptions on initial atmospheric CO_2 concentrations, oceanic nutrient inventory and surface ocean saturation state add only minor additional uncertainty to emission rates (see sensitivity studies in Appendix D). The model results imply isotopically light carbon input (mean composition across all scenarios = −42‰) at the start of the negative CIE (46–50 m) for all scenarios. Toward the peak of the negative CIE, our model results indicate a shift towards the input of less ^{13}C-depleted carbon with a mean composition of −6‰ between 55.5–60.0 m. Additional sensitivity studies (see Appendix D) demonstrate that the necessity for ^{13}C-depleted carbon at the start of the negative CIE is a robust result considering uncertainties in initial atmospheric CO_2 concentration, initial oceanic nutrient inventory, initial carbonate saturation state, and different biological production schemes (temperature-dependent or -independent production).

In our simulations the calcite saturation state (Ω) of the surface ocean only decreases appreciably in experiments with carbon emission rates of at least 0.1 Pg C yr^{-1} (see fig. F1 in Appendix F). In scenarios with slower carbon emissions, surface ocean Ω stays constant or increases slightly. The total Ω change and the associated uncertainty intervals vary between locations and are largest in the tropics (up to ∼-2.5 in the most extreme experiments, see fig. F2 in Appendix F). Sea surface temperature (SST) changes are more variable with pCO_2 change scenario than assumed CIE onset duration, and are largest around Antarctica (see fig. F3 in Appendix F).

The new Os data from Cau (see Fig. 3) show a low concentration of Os with a slight trend towards more radiogenic values (∼1) towards the start of the negative CIE (40–45 m). This is followed by increasing Os concentration during the CIE, its isotopic composition shifting to less radiogenic values (<0.4). A brief excursion back to low concentrations of very radiogenic Os (>1.2) half way through the negative CIE onset (∼55 m) is based on two data points. All data can be found in Appendix E.

4. Discussion

Our inverse modelling suggests that the addition of ^{13}C-depleted carbon during the start of the negative CIE (Phase A in Fig. 4), followed by sustained input of carbon with a largely volcanic isotopic signature (Phase B, typically between −5 and −8‰ away from subduction zones (Javoy et al., 1986)), reconciles the measured $\delta^{13}C_{carb}$ and reconstructed pCO_2 at Cau (Naafs et al., 2016). Our method results in required 'net' carbon fluxes and their isotopic compositions. While we cannot exclude mixes of sources (and sinks) that sum to the right 'net' values, this provides information about the dominant carbon source. The requirement for initial carbon emissions more ^{13}C-depleted than volcanic CO_2 across our simulations indicates that contribution from organic carbon sources (typically between −10 and −30‰ (e.g. Meyers, 1994)) and methane, the only surficial carbon with a $\delta^{13}C < -40$‰, was necessary to drive the CIE at the OAE 1a onset (see Fig. 2b,d and Appendix). Predominant methane emissions, however, are only required in scenarios with minimal pCO_2 rise during the CIE onset. All scenarios require the most ^{13}C-depleted carbon input between 48 m and 52 m. The isotopic composition of the carbon input predicted by cGENIE between 52 m and 58 is consistently less depleted (around or above −10‰ for most simulations) almost regardless of uncertainty in reconstructed pCO_2 or duration. This is consistent only with an appreciable contribu-

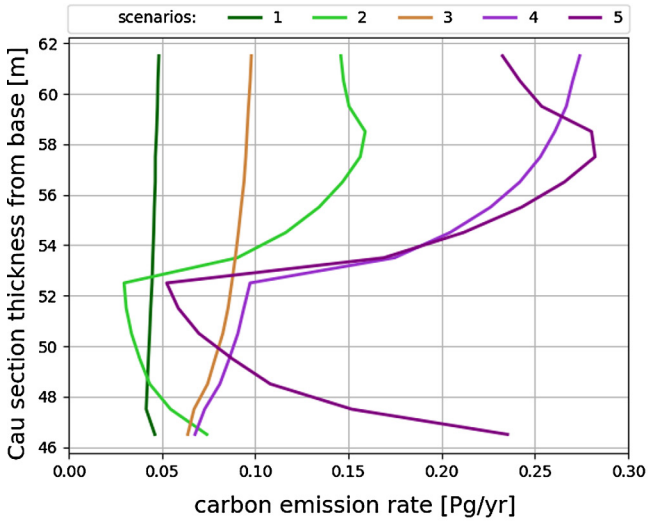

a) carbon mass fluxes across stage C3

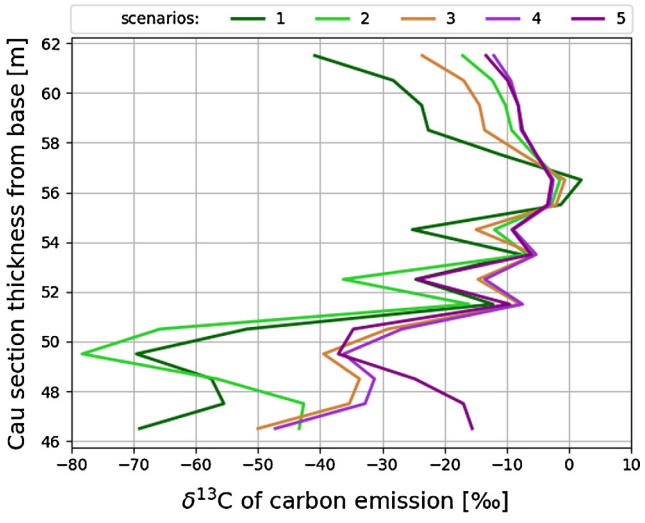

b) δ^{13}C of carbon fluxes

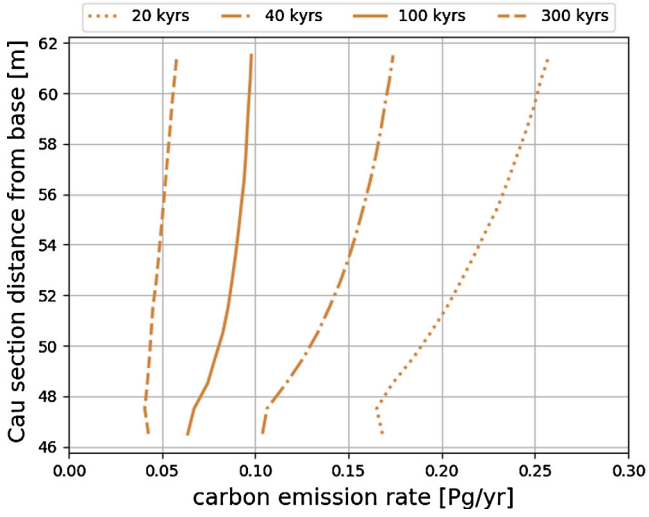

c) carbon masses with different C3 duration estimates

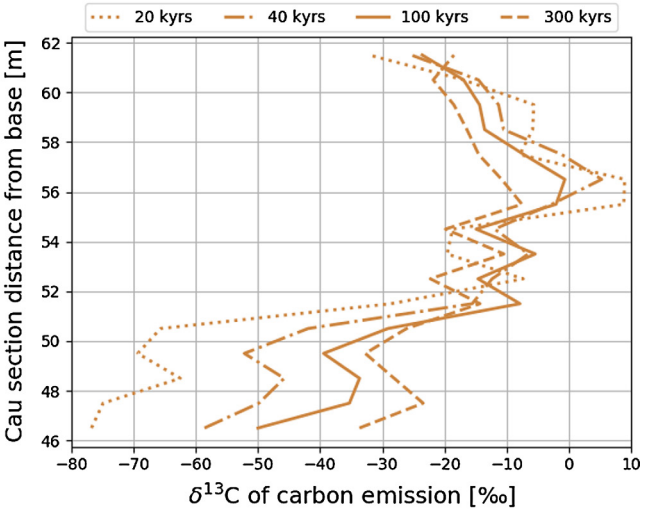

d) δ^{13}C with different duration estimates

Fig. 2. Carbon fluxes and their isotopic signatures across the onset of the negative CIE as calculated by cGENIE. (a) and (b) show differences due to different pCO_2 change scenarios (see Fig. 1), all assuming a CIE onset duration of 100 kyr. (c) and (d) show the influence of a different CIE onset duration (20–300 kyr) examplarily for scenario 3. The results are averaged over 1 m depth equivalent.

tion from a volcanic source. The shift in source from sedimentary organic carbon to volcanism occurs relatively rapidly, within 4 m at Cau or 25 kyr assuming a negative CIE onset duration of 100 kyr and a constant sedimentation rate. Importantly, this difference in isotopic composition between strata below and above 52 m is a robust feature in all simulations and suggests that Earth's system transitioned from predominant input from an isotopically light carbon source to a heavier one. Scenarios with low pCO_2 increase require another pulse of biogenic CO_2 to reach the lowest δ^{13}C values at the end of our simulations, while the isotopic signature of carbon inputs in scenarios with higher emission rates remains close to mantle values.

A shift to a more mantle-like source is supported by published Os isotope data which have been used to infer changes in volcanic activity across OAEs, given that the main source of unradiogenic Os is mantle material (Turgeon and Creaser, 2008; Bottini et al., 2012; Du Vivier et al., 2014). Published OAE 1a Os isotope records from pelagic sections show a shift towards unradiogenic (mantle-like) values during the negative CIE at the onset of OAE 1a (Bottini et al., 2012), suggesting a strengthened Os flux from the mantle. While a direct comparison between Os records from Cau and other sites is hampered by uncertainties in age models and missing stratigraphic ties, records from all sites show similar features. The consistent shift to very unradiogenic Os-isotope values in the Cau record (Fig. 4) is similar to that recorded in other sections and adds confidence to the assumption that strengthened volcanism was the primary control on Os isotope changes recorded across the negative CIE at Cau, even more so given the small amount of preserved organic matter preserved and its platform setting. Similar to other Tethyan sections, the Os record at Cau shows a shift back to radiogenic values before stagnating at unradiogenic values (in phase B in Fig. 4 (Jenkyns, 2018)). Since this excursion is not evident in records from all OAE 1a sections, it might represent a local or regional change with little implications for the reconstructed volcanic strength. In that case the shifts from less to more mantle-like compositions of Os and carbon coincide at Cau (Fig. 4). If the radiogenic excursion at ~55 m in the Cau section reflects a global change of Os fluxes, the resolution of the pCO_2 reconstruction is

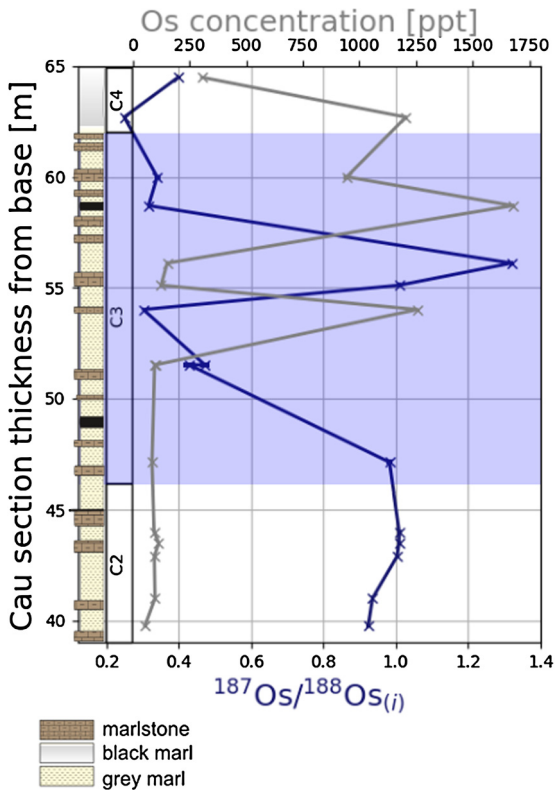

Fig. 3. Os concentration and $^{187}Os/^{188}Os_{(i)}$ between meters 39 and 65 of the Cau section. The onset of the negative CIE is marked by blue shading. Uncertainties on data are smaller than the symbols.

either too coarse to evidence a short-term decline in volcanic carbon emissions, or the relationship between carbon and Os isotopic changes during the onset of LIP emplacement is more complex. At this moment, we cannot test this relationship at other sites because combined records of Os isotope and inferred pCO_2 changes are not available at the required resolution.

Emissions of carbon from an organic matter reservoir are needed to explain carbon isotopic changes at Cau regardless of the pCO_2 scenario or assumed duration of CIE onset. However the exact mechanism of its release at the onset of OAE 1a is not clear. It is unlikely that depleted carbon was emitted due to feedback mechanisms in response to a warming climate (e.g. destabilized methane hydrates), given the small changes in atmospheric pCO_2 at that time. There is, however, evidence in support of geologically-triggered emissions of ^{13}C-depleted organic carbon during the onset of OAE 1a. Polteau et al. (2016) showed that magma intrusions into overlying sediments during the formation of the Barents Sea Sill Complex in the early Aptian could have destabilized a considerable mass of organic carbon and led to thermogenic methane emissions. OAE 1a happened at a time of high magmatic activity, including the emplacement phases of the Ontong-Java Plateau LIP (e.g. Larson and Erba, 1999). We therefore suggest that at the start of the negative CIE magmatic activity increased under thin crust, intruding into organic-rich marine sediments and causing small releases of ^{13}C-depleted thermogenic gases. This initial phase of increased mantle activity was then followed by a more eruptive phase of LIP emplacement, when large-scale submarine volcanism dominated exogenic carbon emissions and delivered large amounts of new mantle material to the ocean floor. This increased the flux of unradiogenic Os into the ocean through hydrothermal vents as well as weathering of fresh basalt and released vast amounts of mantle-sourced carbon to the atmosphere. Thus, the initial $\delta^{13}C$ decrease and the excursions in Os isotopes and $\Delta^{13}C$ are consistent with a scenario in which the recorded CIE and pCO_2 change occured independently: The first through release of sedimentary organic carbon, and the latter through volcanic CO_2 emissions.

Our results based on records of atmospheric pCO_2 and $\delta^{13}C$ are consistent with published model interpretations of Os isotope profiles, which also find that volcanism was the primary carbon source during OAE 1a (Bauer et al., 2017). The mass of emitted carbon in our results is however different from that reconstructed by Bauer et al. (2017) using Os isotopes. The biomarker-based estimate suggests an increase in pCO_2 of 200–1700 ppm (Naafs et al., 2016), whereas the model interpretation of $^{187}Os/^{188}Os$ implies that pCO_2 rose by about 3,000 ppm (Bauer et al., 2017). We tested the implications for carbon sources assuming a continuous CO_2 concentration increase of 3000 ppm, which resulted in increased carbon emissions (0.32 Pg C yr^{-1} assuming a 100 kyr duration, see fig. D4 in the appendix) compared to our scenarios, with isotopic compositions between −20 and −3‰. This is still consistent with a predominantly volcanic source, but reduced the need for more ^{13}C-depleted organic carbon release. Temperature proxy records across OAE 1a (Mutterlose et al., 2014; Naafs and Pancost, 2016) are consistent with regional temperature changes of 1–5 °C produced by scenarios based on the Naafs et al. (2016) pCO_2 reconstruction. The higher (Os based) pCO_2 changes result in a temperature rise of 7 °C globally in cGENIE, equivalent to 5–6 °C in the Tethys which is at the upper end of reconstructed temperature change.

Organic carbon burial is not simulated by our model, meaning that we have to assume that organic carbon burial did not strengthen significantly during the negative CIE onset. Although carbon contents at Cau and at other locations only increase during the recovery of the negative CIE and start of the positive CIE (generally referred to as segments C4-C6 Menegatti et al., 1998; Quijano et al., 2012; Erba et al., 2015), it is unknown to what degree the marine carbon and Os cycles were influenced by organic matter burial locally and/or globally. Widespread organic carbon burial would shorten the residence time of Os and carbon in the ocean and create a sink for ^{12}C, increasing carbon emission rates needed to produce the observed environmental changes. The results from our experiments should thus be regarded as a low-end estimate of the mass of emitted carbon. However, our experiments indicate that the transition from more ^{13} depleted organic carbon input (potentially from sill intrusions) to mantle-sourced carbon (volcanism) is robust against changes in emission rate and total mass of emitted carbon and hence should be detectable despite changes in the amount of organic matter burial.

In terms of timing, high-resolution temperature records (based on palynology and $\delta^{18}O$) at the expanded pelagic section of Pusiano and the shelf section at La Bédoule (Keller et al., 2011; Lorenzen et al., 2013) indicate a time lag between the start of the negative CIE and the main period of warming. This would be consistent with our reconstructed emissions scenarios. At pelagic sections lower sediment accumulation rates and coarser sampling resolutions (e.g. Cismon, Roter Sattel, Pacific DSDP site 463 and Atlantic DSDP site 398), likely prevented the identification of such time lag between temperature proxies and negative CIE (Menegatti et al., 1998; Ando et al., 2008; Naafs and Pancost, 2016).

Major changes in the marine nannofossil community, including dwarfism, and a decline in $CaCO_3$ burial rates, have been observed during the negative CIE and interpreted as an indicator for a decline in calcite surface ocean saturation state due to large carbon emissions (Weissert and Erba, 2004; Erba et al., 2010). The widespread occurrence of surface ocean acidification during OAE 1a as driver of biological turn-over is contested (Gibbs et al., 2011; Naafs et al., 2016). Our simulations show that only scenarios with a large carbon source or short event duration result in an appreciable Ω decline ($\Delta\Omega > 0.5$), globally and locally. A decrease in

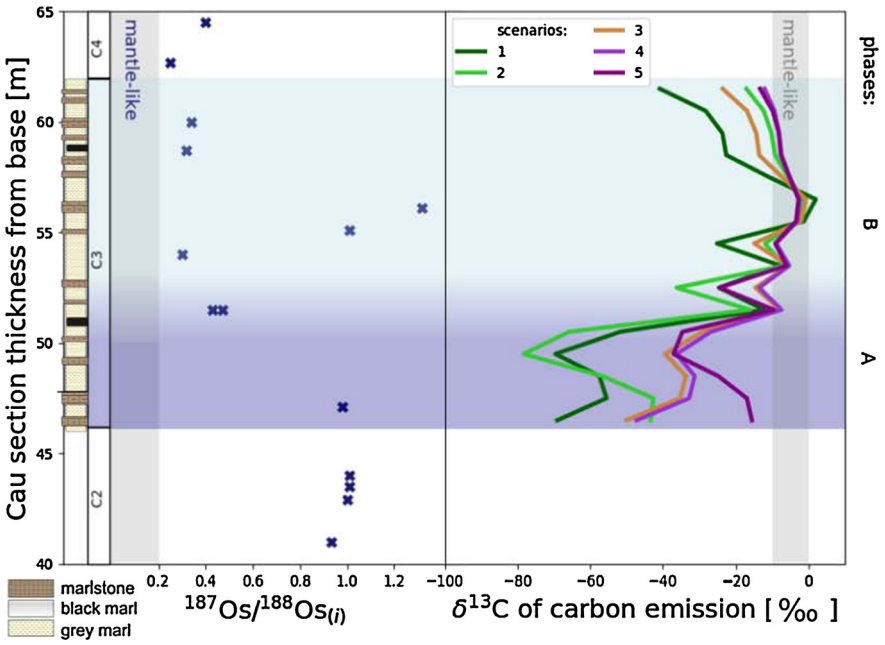

Fig. 4. Osmium isotopic changes (left) and reconstructed $\delta^{13}C$ signature of emissions based on carbon isotopes (right) at Cau. The two shaded sections show phases of least (A) and most prominent (B) volcanic activity.

saturation state could have imposed significant stress onto calcifiers (Weissert and Erba, 2004). At Cau, the pCO_2 changes and the decline in Ω (around 54 m) began well after the onset of the nannofossil decline, which starts at ∼43 m. In our longer simulations (≥100 kyr) increased weathering and continental runoff eventually counteract the CO_2 dissolution effect, which leads to a recovered or even increased calcite saturation state at the end of these experiments, despite ongoing carbon emissions. Further quantitative comparison of the impact of carbon emissions onto the surface ocean carbonate chemistry in our simulations is hampered by remaining uncertainties. For example, the carbonate system of the pre-OAE 1a Aptian surface ocean is poorly constrained. Particularly the mass of emitted carbon needed to cause appreciable Ω changes and the position of the carbonate compensation depth depend largely on these initial conditions. The slow carbon emission rates predicted by our model are also a function of the duration of the negative CIE onset. Unless the onset took 20 kyr (Malinverno et al., 2010, the smallest current estimate) or less, it is unlikely that carbon emissions could have outpaced the weathering feedbacks that stabilize the surface ocean saturation state (Hönisch et al., 2012). As such, estimated onset durations and the temporal decoupling between changes in calcite saturation state and nannoconid crisis make it unlikely that this major perturbation of the marine nanno-calcifier community was a direct result of carbon emissions driving the negative CIE.

5. Conclusion

We used transient model simulations based on combined pCO_2 and $\delta^{13}C$ records to identify dominant carbon sources and quantify associated emission rates. The simulations show that carbon emission rates of 0.043–1.46 Pg C yr^{-1} reconcile the negative CIE and pCO_2 estimates, with the exact rate depending on the assumed duration of OAE onset. Assuming a baseline pCO_2 of 850 ppm this is consistent with estimates of moderate temperature change from diverse proxy data. Our results suggest that an initial input of predominantly ^{13}C-depleted carbon was responsible for the negative CIE associated with OAE 1a, but had little effect on atmospheric pCO_2. This carbon could have originated from sill intrusions into marine organic rich sediments, potentially releasing thermogenic and/or biogenic methane. Following this initial phase, volcanic (less ^{13}C-depleted) carbon emissions sustained the stagnant part of the negative CIE and fuelled most of the recorded atmospheric pCO_2 increase. Our results indicate that organic carbon emissions in form of methane and/or CO_2, despite shaping the $\delta^{13}C$ curve, did not increase the atmospheric carbon reservoir appreciably. Importantly, this demonstrates that the scale and nature of the Earth system perturbation at the onset of OAE 1a cannot be determined based on the existence of a negative CIE or its size alone. This may also be the case for other negative CIEs in the geological record. Our results further imply the possibility of a time lag between the carbon isotopic excursion and the major phase of carbon emissions, but highly resolved records from other sections are necessary to corroborate this finding. Uncertainties in the amount of atmospheric pCO_2 change and duration of the OAE onset create proportionally large uncertainties on carbon emission rates and their initial isotopic composition. Increased accuracy in duration and pCO_2 change estimates are needed to narrow down our estimates of carbon flux magnitudes and origins. However, the shift from more to less ^{13}C-depleted carbon emissions is robust against these uncertainties, as are the pure volcanic-like carbon fluxes towards the peak of the negative CIE. We conclude that mantle activity increased in the early Aptian, heating organic-rich marine sediments and releasing thermogenic methane before sustained mantle eruptions led to OAE formation.

Data availability

All Os and Re measurements are provided in the Supplementary Material. The model source code and instructions on how to repeat the simulations presented in this manuscript can be accessed as stated under 'Code availability'. Specific simulation outputs can be obtained from Markus Adloff.

Code availability

muffin overview

The code for the cGENIE.muffin model is hosted on GitHub. The current version can be obtained by cloning:

https://github.com/derpycode/cgenie.muffin

A manual, detailing code installation, basic model configuration, plus an extensive series of tutorials covering various aspects of muffin capability, experimental design, and results output and processing, is provided. A PDF of the manual can be downloaded here:

http://www.seao2.info/cgenie/docs/muffin.pdf

The latex source and most up-to-date built PDF file can be obtained by cloning:

https://github.com/derpycode/muffindoc

Instructions summary

The muffin manual contains instructions for obtaining, installing, and testing the code, plus how to run experiments. Specifically:

Section 1.1 – provides a basic over-view of the software environment required for installing and running muffin.
Section 1.2.2 – provides a basic over-view of cloning and testing the code.
Secion 15.4 – provides a detailed guide to cloning the code and configuring a Ubuntu (18.04) software environment including netCDF library installation, plus running a basic test.
Secion 15.6 – provides a detailed guide to cloning the code and configuring a macOS software environment including netCDF library installation, plus running a basic test.
Secion 1.3 – provides a basic guide to running experiments (also see 1.6 and 1.7).
Secion 1.4 – provides a basic introduction to model output (much more detail is given in Section 12).

Model experiments

Configuration files for the specific experiments presented in the paper can be found in the directory:

`cgenie.muffin\genie-userconfigs\MS\adloffetal.2019`

Details of the different experiments, plus the command line needed to run each one, are given in `readme`.txt.

Declaration of competing interest

We wish to confirm that there are no known conflicts of interest associated with this publication and there has been no significant financial support for this work that could have influenced its outcome.

We confirm that the manuscript has been read and approved by all named authors and that there are no other persons who satisfied the criteria for authorship but are not listed. We further confirm that the order of authors listed in the manuscript has been approved by all of us.

We confirm that we have given due consideration to the protection of intellectual property associated with this work and that there are no impediments to publication, including the timing of publication, with respect to intellectual property. In so doing we confirm that we have followed the regulations of our institutions concerning intellectual property.

Acknowledgements

We would like to thank Stephen Hesselbo and Sandra Kirtland Turner for helpful discussions of, and comments on, the study design. We also want to acknowledge the constructive comments by two anonymous reviewers, which helped us to improve the manuscript.

Furthermore, we would like to thank our funding bodies: M.A. was supported by the NERC GW4+ DTP and the NERC grant NE/L002434/1. S.E.G. was supported by NERC grants NE/L011050/1 and NE/P01903X/1 while working on this manuscript. FMM was supported by a NERC research fellowship (NE/J019062/1) and a NERC standard grant (NE/N011112/1). B.D.A.N. was funded through a Royal Society Tata University Research Fellowship. W.P. was supported by ERC Grant Agreement no. 340923. J.M.C. has received funding from the Spanish Ministry of Science and Technology (project CGL2014-55274-P) and Research Group RNM-200 (Junta de Andalucía).

Appendix A. Supplementary material

Supplementary material related to this article can be found online at https://doi.org/10.1016/j.epsl.2019.115947.

References

Aguado, R., Castro, J.M., Company, M., De Gea, G.A., 1999. Aptian bio-events—an integrated biostratigraphic analysis of the Almadich Formation, Inner Prebetic Domain, SE Spain. Cretac. Res. 20, 663–683.
Ando, A., Kaiho, K., Kawahata, H., Kakegawa, T., 2008. Timing and magnitude of early Aptian extreme warming: unraveling primary $\delta^{18}O$ variation in indurated pelagic carbonates at Deep Sea Drilling Project Site 463, central Pacific Ocean. Palaeogeogr. Palaeoclimatol. Palaeoecol. 260, 463–476.
Bauer, K.W., Zeebe, R.E., Wortmann, U.G., 2017. Quantifying the volcanic emissions which triggered Oceanic Anoxic Event 1a and their effect on ocean acidification. Sedimentology 64, 204–214.
Beerling, D.J., Lomas, M., Gröcke, D.R., 2002. On the nature of methane gas-hydrate dissociation during the Toarcian and Aptian oceanic anoxic events. Am. J. Sci. 302, 28–49.
Birck, J.L., Barman, M.R., Capmas, F., 1997. Re-Os isotopic measurements at the femtomole level in natural samples. Geostand. Newsl. 21, 19–27.
Bottini, C., Cohen, A.S., Erba, E., Jenkyns, H.C., Coe, A.L., 2012. Osmium-isotope evidence for volcanism, weathering, and ocean mixing during the early Aptian OAE 1a. Geology 40, 583–586.
van Breugel, Y., Schouten, S., Tsikos, H., Erba, E., Price, G.D., Sinninghe Damsté, J.S., 2007. Synchronous negative carbon isotope shifts in marine and terrestrial biomarkers at the onset of the early Aptian oceanic anoxic event 1a: evidence for the release of ^{13}C-depleted carbon into the atmosphere. Paleoceanography 22, PA1210.
Castro, J., De Gea, G., Ruiz-Ortiz, P., Nieto, L., 2008. Development of carbonate platforms on an extensional (rifted) margin: the Valanginian–Albian record of the Prebetic of Alicante (SE Spain). Cretac. Res. 29, 848–860.
Colbourn, G., Ridgwell, A., Lenton, T., 2013. The rock geochemical model (rokgem) v0. 9. Geosci. Model Dev. 6, 1543–1573.
Craig, H., 1953. The geochemistry of the stable carbon isotopes. Geochim. Cosmochim. Acta 3, 53–92.
Cui, Y., Kump, L.R., Ridgwell, A.J., Charles, A.J., Junium, C.K., Diefendorf, A.F., Freeman, K.H., Urban, N.M., Harding, I.C., 2011. Slow release of fossil carbon during the Palaeocene–Eocene Thermal Maximum. Nat. Geosci. 4, 481.
Donnadieu, Y., Pierrehumbert, R., Jacob, R., Fluteau, F., 2006. Modelling the primary control of paleogeography on Cretaceous climate. Earth Planet. Sci. Lett. 248, 426–437.
Du Vivier, A.D., Selby, D., Sageman, B.B., Jarvis, I., Gröcke, D.R., Voigt, S., 2014. Marine $^{187}Os/^{188}Os$ isotope stratigraphy reveals the interaction of volcanism and ocean circulation during Oceanic Anoxic Event 2. Earth Planet. Sci. Lett. 389, 23–33.
Edwards, N.R., Marsh, R., 2005. Uncertainties due to transport-parameter sensitivity in an efficient 3-D ocean-climate model. Clim. Dyn. 24, 415–433.
Erba, E., Bottini, C., Weissert, H.J., Keller, C.E., 2010. Calcareous nannoplankton response to surface-water acidification around Oceanic Anoxic Event 1a. Science 329, 428–432.
Erba, E., Duncan, R.A., Bottini, C., Tiraboschi, D., Weissert, H., Jenkyns, H.C., Malinverno, A., 2015. Environmental consequences of Ontong Java Plateau and Kerguelen Plateau volcanism. The origin, evolution, and environmental impact of oceanic large igneous provinces. Spec. Pap., Geol. Soc. Am. 511, 271–303.
Gibbs, S.J., Robinson, S.A., Bown, P.R., Jones, T.D., Henderiks, J., 2011. Comment on "Calcareous nannoplankton response to surface-water acidification around Oceanic Anoxic Event 1a". Science 332, 175.
Gutjahr, M., Ridgwell, A., Sexton, P.F., Anagnostou, E., Pearson, P.N., Pälike, H., Norris, R.D., Thomas, E., Foster, G.L., 2017. Very large release of mostly volcanic carbon during the Palaeocene–Eocene Thermal Maximum. Nature 548, 573.
Hönisch, B., Ridgwell, A., Schmidt, D.N., Thomas, E., Gibbs, S.J., Sluijs, A., Zeebe, R., Kump, L., Martindale, R.C., Greene, S.E., et al., 2012. The geological record of ocean acidification. Science 335, 1058–1063.

Hu, X., Zhao, K., Yilmaz, I.O., Li, Y., 2012. Stratigraphic transition and palaeoenvironmental changes from the Aptian oceanic anoxic event 1a (OAE1a) to the oceanic red bed 1 (ORB1) in the Yenicesihlar section, central Turkey. Cretac. Res. 38, 40–51.

Javoy, M., Pineau, F., Delorme, H., 1986. Carbon and nitrogen isotopes in the mantle. Chem. Geol. 57, 41–62.

Jenkyns, H.C., 2010. Geochemistry of oceanic anoxic events. Geochem. Geophys. Geosyst. 11, Q03004.

Jenkyns, H.C., 2018. Transient cooling episodes during Cretaceous Oceanic Anoxic Events with special reference to OAE 1a (Early Aptian). Philos. Trans. R. Soc. A, Math. Phys. Eng. Sci. 376, 20170073.

John, E.H., Wilson, J.D., Pearson, P.N., Ridgwell, A., 2014. Temperature-dependent remineralization and carbon cycling in the warm Eocene oceans. Palaeogeogr. Palaeoclimatol. Palaeoecol. 413, 158–166.

Josso, P., Parkinson, I., Horstwood, M., Lusty, P., Chenery, S., Murton, B., 2019. Complementarity of Co-chronometry, LA-ICP-MS and Os isotopes for the development of composite age model for deep-ocean ferromanganese crust. Chem. Geol. 513, 108–119.

Keller, C.E., Hochuli, P.A., Weissert, H., Bernasconi, S.M., Giorgioni, M., Garcia, T.I., 2011. A volcanically induced climate warming and floral change preceded the onset of OAE1a (Early Cretaceous). Palaeogeogr. Palaeoclimatol. Palaeoecol. 305, 43–49.

Kirtland-Turner, S., Ridgwell, A., 2016. Development of a novel empirical framework for interpreting geological carbon isotope excursions, with implications for the rate of carbon injection across the PETM. Earth Planet. Sci. Lett. 435, 1–13.

Larson, R.L., Erba, E., 1999. Onset of the Mid-Cretaceous greenhouse in the Barremian-Aptian: Igneous events and the biological, sedimentary, and geochemical responses. Paleoceanography 14, 663–678.

Li, Y.-X., Bralower, T.J., Montañez, I.P., Osleger, D.A., Arthur, M.A., Bice, D.M., Herbert, T.D., Erba, E., Silva, I.P., 2008. Toward an orbital chronology for the early Aptian oceanic anoxic event (OAE1a, ~120 Ma). Earth Planet. Sci. Lett. 271, 88–100.

Lorenzen, J., Kuhnt, W., Holbourn, A., Flögel, S., Moullade, M., Tronchetti, G., 2013. A new sediment core from the Bedoulian (Lower Aptian) stratotype at Roquefort-La Bédoule, SE France. Cretac. Res. 39, 6–16.

Malinverno, A., Erba, E., Herbert, T., 2010. Orbital tuning as an inverse problem: chronology of the early Aptian oceanic anoxic event 1a (Selli Level) in the Cismon APTICORE. Paleoceanography 25, PA2203.

Méhay, S., Keller, C.E., Bernasconi, S.M., Weissert, H., Erba, E., Bottini, C., Hochuli, P.A., 2009. A volcanic CO_2 pulse triggered the Cretaceous Oceanic Anoxic Event 1a and a biocalcification crisis. Geology 37, 819–822.

Menegatti, A.P., Weissert, H., Brown, R.S., Tyson, R.V., Farrimond, P., Strasser, A., Caron, M., 1998. High-resolution $\delta^{13}C$ stratigraphy through the early Aptian "Livello Selli" of the Alpine Tethys. Paleoceanography 13, 530–545.

Meyers, P.A., 1994. Preservation of elemental and isotopic source identification of sedimentary organic matter. Chem. Geol. 114, 289–302.

Miller, C.A., Peucker-Ehrenbrink, B., Ball, L., 2009. Precise determination of rhenium isotope composition by multi-collector inductively-coupled plasma mass spectrometry. J. Anal. At. Spectrom. 24, 1069–1078.

Monteiro, F.M., Pancost, R.D., Ridgwell, A., Donnadieu, Y., 2012. Nutrients as the dominant control on the spread of anoxia and euxinia across the Cenomanian-Turonian oceanic anoxic event (OAE2): model-data comparison. Paleoceanography 27, PA4209.

Mutterlose, J., Bottini, C., Schouten, S., Sinninghe Damsté, J.S., 2014. High sea-surface temperatures during the early Aptian Oceanic Anoxic Event 1a in the Boreal Realm. Geology 42, 439–442.

Naafs, B., Castro, J., De Gea, G., Quijano, M., Schmidt, D., Pancost, R., 2016. Gradual and sustained carbon dioxide release during Aptian Oceanic Anoxic Event 1a. Nat. Geosci. 9, 135–139.

Naafs, B., Pancost, R., 2016. Sea-surface temperature evolution across Aptian Oceanic Anoxic Event 1a. Geology 44, 959–962.

Olierook, H.K., Jourdan, F., Merle, R.E., 2019. Age of the Barremian–Aptian boundary and onset of the Cretaceous Normal Superchron. Earth-Sci. Rev., 102906.

Polteau, S., Hendriks, B.W., Planke, S., Ganerød, M., Corfu, F., Faleide, J.I., Midtkandal, I., Svensen, H.S., Myklebust, R., 2016. The Early Cretaceous Barents Sea sill complex: distribution, $^{40}Ar/^{39}Ar$ geochronology, and implications for carbon gas formation. Palaeogeogr. Palaeoclimatol. Palaeoecol. 441, 83–95.

Popp, B.N., Laws, E.A., Bidigare, R.R., Dore, J.E., Hanson, K.L., Wakeham, S.G., 1998. Effect of phytoplankton cell geometry on carbon isotopic fractionation. Geochim. Cosmochim. Acta 62, 69–77.

Quijano, M.L., Castro, J.M., Pancost, R.D., de Gea, G.A., Najarro, M., Aguado, R., Rosales, I., Martín-Chivelet, J., 2012. Organic geochemistry, stable isotopes, and facies analysis of the Early Aptian OAE—New records from Spain (Western Tethys). Palaeogeogr. Palaeoclimatol. Palaeoecol. 365, 276–293.

Ridgwell, A., Hargreaves, J., 2007. Regulation of atmospheric CO_2 by deep-sea sediments in an Earth system model. Glob. Biogeochem. Cycles 21, GB2008.

Ridgwell, A., Hargreaves, J., Edwards, N.R., Annan, J., Lenton, T.M., Marsh, R., Yool, A., Watson, A., 2007. Marine geochemical data assimilation in an efficient Earth System Model of global biogeochemical cycling. Biogeosciences 4, 87–104.

Ridgwell, A., Schmidt, D.N., 2010. Past constraints on the vulnerability of marine calcifiers to massive carbon dioxide release. Nat. Geosci. 3, 196.

Ridgwell, A., Zeebe, R.E., 2005. The role of the global carbonate cycle in the regulation and evolution of the Earth system. Earth Planet. Sci. Lett. 234, 299–315.

Schlanger, S.O., Jenkyns, H., 1976. Cretaceous oceanic anoxic events: causes and consequences. Neth. J. Geosci./Geol. Mijnb. 55, 179–184.

Shirey, S.B., Walker, R.J., 1995. Carius tube digestion for low-blank rhenium-osmium analysis. Anal. Chem. 67, 2136–2141.

Tejada, M.L.G., Suzuki, K., Kuroda, J., Coccioni, R., Mahoney, J.J., Ohkouchi, N., Sakamoto, T., Tatsumi, Y., 2009. Ontong Java Plateau eruption as a trigger for the early Aptian oceanic anoxic event. Geology 37, 855–858.

Turgeon, S.C., Creaser, R.A., 2008. Cretaceous oceanic anoxic event 2 triggered by a massive magmatic episode. Nature 454, 323.

Turner, S.K., Ridgwell, A., 2013. Recovering the true size of an Eocene hyperthermal from the marine sedimentary record. Paleoceanography 28, 700–712.

Wang, Y., Huang, C., Sun, B., Quan, C., Wu, J., Lin, Z., 2014. Paleo-CO_2 variation trends and the Cretaceous greenhouse climate. Earth-Sci. Rev. 129, 136–147.

Weissert, H., 1989. C-isotope stratigraphy, a monitor of paleoenvironmental change: a case study from the Early Cretaceous. Surv. Geophys. 10, 1–61.

Weissert, H., Erba, E., 2004. Volcanism, CO_2 and palaeoclimate: a Late Jurassic–Early Cretaceous carbon and oxygen isotope record. J. Geol. Soc. 161, 695–702.

Wissler, L., Funk, H., Weissert, H., 2003. Response of early Cretaceous carbonate platforms to changes in atmospheric carbon dioxide levels. Palaeogeogr. Palaeoclimatol. Palaeoecol. 200, 187–205.